Assessment of short-range forecast error atmosphere-ocean cross-correlations from the Met Office coupled numerical weather prediction system

Article

Published Version

It is advisable to refer to the publisher's version if you intend to cite from the work. See Guidance on citing.

To link to this article DOI: http://dx.doi.org/10.1002/qj.4735

the End User Agreement.

www.reading.ac.uk/centaur

CentAUR

Central Archive at the University of Reading

Reading's research outputs online

RESEARCH ARTICLE

Assessment of short-range forecast error atmosphere–ocean cross-correlations from the Met Office coupled numerical weather prediction system

Azin Wright[1] | Amos S. Lawless[1,2] | Nancy K. Nichols[1,2] | Daniel J. Lea[3] | Matthew J. Martin[3]

[1]School of Mathematical, Physical and Computational Sciences, University of Reading, Reading, UK

[2]National Centre for Earth Observation, Reading, UK

[3]Ocean Forecasting Research and Development, Met Office, Exeter, UK

Correspondence
Amos S. Lawless, Department of Mathematics and Statistics, University of Reading, Pepper Lane, Whiteknights, Reading, RG6 6AX, UK.
Email: a.s.lawless@reading.ac.uk

Abstract

Operational data assimilation systems for coupled atmosphere–ocean prediction are usually "weakly coupled", in which there is no explicit interaction between the atmosphere and ocean within the data assimilation step. Explicitly allowing for cross-correlations between the ocean and the atmosphere may have potential benefits in improving the consistency of atmosphere and ocean analyses, as well as allowing a better use of observations at the interface. To understand whether such correlations are significant on the time-scales of numerical weather prediction, we investigate the atmosphere–ocean cross-correlations of short-term forecast errors from the Met Office coupled prediction system, considering their temporal and spatial variability. We find that significant correlations exist between atmosphere and ocean forecast errors on these time-scales, and that these vary diurnally, from day to day, spatially and synoptically. For correlations between errors in the atmospheric wind and ocean temperature, positive correlations in the North Atlantic region are found to be synoptically dependent, with correlation structures extending into the ocean throughout the deep mixed layer, beyond a depth of 100 m. In contrast, negative correlations over the Indian Ocean are very shallow and are associated with the diurnal cycle of solar radiation. The significance and variability of cross-correlations indicates that there should be a benefit from including them in data assimilation systems, but it will be important to allow for some flow-dependence in the correlations. Furthermore, the differing vertical extents of the cross-correlations in different regions implies the need for situation-dependent localisation of ensemble correlations when including them in coupled data assimilation systems.

KEYWORDS
air–sea coupling, background-error covariances, coupled data assimilation, cross-covariances, variational data assimilation

1 | INTRODUCTION

Many atmospheric phenomena are tightly coupled to ocean processes, and the correct forecasting of these phenomena relies on a good representation of atmosphere–ocean interactions (Vellinga *et al.*, 2020). A clear example of this is the prediction of the formation and development of tropical cyclones, which depends strongly on correctly capturing the transfer of ocean heat into the atmosphere. In order to improve the forecasting of such events, many operational numerical weather prediction (NWP) centres have recently been moving towards using coupled models in their forecasting systems, in which different components of the Earth system can interact with each other. The use of these coupled models for weather prediction requires their careful initialisation, to avoid imbalances arising at the interfaces between different components. Hence, new developments in coupled data assimilation (CDA) are required.

At the Met Office and the European Centre for Medium-range Weather Forecasts (ECMWF), coupled atmosphere–ocean systems are now used for routine operational forecasts. Both of these centres use variational data assimilation (DA) to initialise their models and have based their CDA systems on weakly-coupled DA within the incremental variational assimilation framework. In the weakly coupled method the inner-loop assimilation step is performed separately for the atmosphere and ocean to find the analysis increments. The full, coupled model is used to cycle between assimilation times, providing the background information for the next assimilation window (Browne *et al.*, 2019; de Rosnay *et al.*, 2022). This background may also be used to calculate the innovations for the new assimilation window, as is done in the Met Office weakly-coupled DA system that we use in this study (Lea *et al.*, 2015, 2022). Compared with strongly-coupled DA, in which CDA is applied to the full, coupled model, the weakly coupled approach is more technically feasible with current operational systems, as it allows the DA software for the atmosphere and ocean to be kept separate and can also allow different DA schemes in the atmosphere and ocean.

Besides producing a more balanced initialisation, an advantage of CDA is that it allows atmosphere observations to influence the analysis of the ocean state and vice versa. Hence, it should lead to a better use of observations at the atmosphere–ocean interface. However, the degree of this influence depends on the specific details of the CDA scheme. Even in cycled weakly-coupled DA, the use of the coupled model allows observations of one fluid to influence the other at the next assimilation time. In a theoretical study using a single-column atmosphere–ocean model, Smith *et al.* (2015) looked at the influence of observations with differing degrees of coupling. They showed that with

a weakly coupled system with just one outer loop there was no communication across the fluid interface at the start of the assimilation window, but the coupled state later in the window is affected by all observations assimilated. However, with multiple outer loops and observations in both fluids, it is possible for information to be transferred across the interface even at the start of the assimilation window. In the ECMWF system, Laloyaux *et al.* (2018) showed that outer-loop coupling was able to produce effective implicit covariances, but that this happened several hours into the assimilation window. They concluded that for short windows there may be less benefit from using multiple outer loops and it may be more useful to specify cross-covariances at the initial time.

Before embarking on the technical work needed to introduce explicit cross-covariances in CDA, it is useful to ask whether strong atmosphere–ocean cross-correlations do exist and, if so, what is the nature of them. In particular, for the purposes of NWP, we are interested in the forecast error correlations that exist on the time-scale of the assimilation window, which is 6 hr for both the atmosphere and ocean in the Met Office CDA scheme. In this study, we investigate the structure of the error correlations on this short time-scale. Furthermore, to understand how we may use such information in NWP, we examine the temporal variation of these correlations, both throughout the day and over a period of days to weeks.

Previous work has examined the nature of atmosphere–ocean cross-covariances in other contexts. In an idealised single-column system Smith *et al.* (2017, 2018) used an ensemble of cycled four-dimensional variational assimilations to calculate correlations between errors in different atmospheric and oceanic variables. They showed that in their system there were strong correlations and that the sign and structure of these could vary seasonally and from day to night. In a later study using the same model, they showed that the explicit use of these covariances allowed a more consistent analysis when either only the atmosphere or only the ocean was observed (Smith *et al.*, 2020). A study of atmosphere–ocean cross-covariances for a more realistic model was performed by Frolov *et al.* (2021), using the coupled model of the US Naval Research Laboratory. They used a 16-member ensemble of their system, with a 1/3°-resolution atmosphere model and a 1/12° (eddy-resolving) ocean model, to calculate covariances over a period of just over 1 year. Their system used a weakly-coupled DA approach, with the atmosphere fields updated every 6 hr and the ocean fields every 24 hr. The study performed an analysis of the covariances between atmosphere and ocean 24-hr forecast anomalies, finding significant correlations in annual-average spatial correlation patterns and the annual cycle of regionally averaged correlations.

Our aim here is to understand the nature of the atmosphere–ocean cross-correlations relevant to NWP as implemented at the Met Office, which uses a 6 hr forecast for the background field. We investigate the structure of these cross-correlations in daily mean fields derived from a sequence of 6 hr forecasts, before looking at the diurnal and synoptic variation of the cross-correlations. We then examine how far the cross-correlations extend vertically into the atmosphere and ocean. We begin the article by describing the Met Office system and outlining our methodology in Section 2. We then present and discuss our results in Section 3 before concluding in Section 4.

2 | METHODOLOGY

We use a development version of the Met Office coupled NWP ensemble system in this article (Lea *et al.*, 2023). The atmosphere, land, ocean, and sea-ice model components are all from an operational version of the system, as are the atmospheric DA, atmospheric ensemble aspects, and the ocean DA. The only aspect that is not yet operational is the ocean ensemble generation methodology, which is described in detail by Lea *et al.* (2022). Here, we summarise the coupled model, CDA, and ensemble generation aspects of the system.

2.1 | Coupled model

The model used in the coupled NWP system is the GC4 configuration of the Met Office coupled modelling system. It consists of the Met Office Unified Model (MetUM) atmospheric model in the GA8 configuration, the Joint UK Land Environment Simulator land-surface model in the GL9 configuration, the Nucleus for European Modelling of the Ocean (NEMO) ocean model in the GO6 configuration (Storkey *et al.*, 2018), and the CICE sea-ice model in the GSI8.1 configuration (Ridley *et al.*, 2018). Earlier versions of the atmosphere and land model components were described by Walters *et al.* (2019), with the following key changes since then: prognostic based entrainment, which adds convective memory and improves precipitation rates and spatial structures; time-smoothed convective increments, which improve the convection–dynamics coupling and greatly reduce the dynamical effects of convective intermittency; a new riming parametrisation, which increases the amount of supercooled water and hence reduces Southern Ocean biases; and a package of surface changes, which improves the forecast of near-surface winds and removes the need for the aggregate tile in NWP. The atmosphere and land are run in one executable, and the ocean and sea ice are run in a second executable.

Hourly coupling fields are exchanged between the two using the OASIS coupler (Craig *et al.*, 2017).

In the operational system the horizontal resolution of the atmosphere and land models is N1280 ($\sim$10 km) for the deterministic forecasts and N640 ($\sim$20 km) for the ensemble forecasts. However, these are very computationally expensive to run, so the experiments described here use lower resolution versions of N640 ($\sim$20 km) for the deterministic forecasts and N320 ($\sim$40 km) for the ensemble forecasts. The model uses a terrain-following height coordinate, with 70 levels in the vertical, of which 50 are below 18 km (Walters *et al.*, 2019). The ocean and sea-ice model horizontal resolution is 1/4° ($\sim$25 km) for both deterministic and ensemble components, both operationally and in the experiments described here. The ocean model has 75 vertical levels, which range in thickness from 1 m near the surface to 300 m at 6,000 m depth.

2.2 | Coupled data assimilation

The atmospheric component of the DA for the deterministic forecasting system is carried out using a hybrid four-dimensional variational approach (Bowler *et al.*, 2017a). This uses a combination of the forecast-error covariances from the global Met Office Global and Regional Ensemble Prediction System (MOGREPS-G) ensemble (described in Section 2.3) with climatological error covariance information. It uses a linear perturbation forecast model to (in effect) evolve the forecast-error covariances through the assimilation window of 6 hr. The land-surface DA uses an extended Kalman filter approach and is described by Gómez *et al.* (2020). The ocean and sea-ice DA are both carried out using a three-dimensional variational "first guess at appropriate time" scheme based on the NEMOVAR code (Mirouze *et al.*, 2016; Waters *et al.*, 2015). The DA for ocean and sea ice are run separately.

These separate atmosphere, land, ocean, and sea-ice DA systems are combined in a coupled DA framework as described by Lea *et al.* (2015) and Guiavarc'h *et al.* (2019). All of the component DA systems are run on a 6 hr cycle where the inputs to the DA, including the innovations (observation-minus-model values in observation space) and nonlinear model trajectory information, come from the coupled model forecast. Separate systems (as just described) are then used to produce the analysis increments for the ocean, sea ice, atmosphere, and land. Note that the sea-ice concentration data assimilated are from a product that collects all data for each day and has a nominal time of 1200 UTC, so only the 1200 UTC cycle includes sea-ice DA. The atmospheric increments are added into the atmospheric component of the coupled

model at the beginning of the time window with direct insertion, whereas the ocean and sea-ice increments are added in using incremental analysis updates (IAU; Bloom *et al.*, 1996) over the first 3 hr of the time window. The analysis is valid in the middle of the time windows (0000, 0600, 1200, 1800 UTC), and forecasts are launched from these times.

2.3 | Coupled ensemble generation

The atmospheric component of the coupled ensemble uses an ensemble of hybrid four-dimensional ensemble variational DAs as described by Inverarity *et al.* (2023). The Mean–Pert method of Lorenc *et al.* (2017) is used to reduce the cost of the ensemble DA (EDA) by generating an accurate analysis of the ensemble mean, with the analyses of the ensemble perturbations carried out using fewer minimisation iterations (and therefore lower computational cost). EDA schemes are either stochastic, which need to perturb observations, or deterministic, which adopt adjusted formulations of the analysis update equation (Houtekamer & Zhang, 2016). The atmospheric EDA takes the latter approach, using the relaxation-to-prior-perturbations technique of Whitaker and Hamill (2012) (the ocean ensemble adopts the former approach, as described later). Ensemble inflation is also used in the atmospheric EDA using the relaxation-to-prior, spread method to account for errors in the DA specifications. Stochastic atmospheric model perturbations are applied in all ensemble member forecasts using the "stochastic kinetic energy backscatter" scheme (Tennant & Beare, 2014) and "stochastic perturbation of tendencies" scheme (Sanchez *et al.*, 2016). An additive inflation scheme (Piccolo *et al.*, 2019) is also used, both to provide additional perturbations to the ensemble forecast and to correct model biases.

The ocean and sea-ice ensemble is initialised using an ensemble of three-dimensional variational first guess at appropriate time analyses. In each member of the ensemble the observations used in the assimilation are perturbed in their values (by the expected measurement error for each observation) and locations (to mimic errors of representation). These observation perturbations were shown by Lea *et al.* (2022) to generate good spread in the different observed variables. Stochastic model perturbations were also included in the NEMO ocean model for each ensemble member based on schemes described by Storto and Andriopoulos (2021). These include a stochastic perturbation of tendencies scheme, which adds a perturbation to the total parametrised physics tendencies that is the product of the unperturbed tendencies and a random field. The "stochastically perturbed parameters" scheme

(Ollinaho *et al.*, 2017) introduces stochastic perturbations to model parameters within parametrised processes. The stochastic kinetic energy backscatter scheme adds perturbations to the barotropic streamfunction proportionally to some sinks of energy on small scales in the model, which in a higher resolution model would otherwise have been backscattered to the scales we can resolve. An assessment of the reliability of the ocean–sea-ice ensemble including the aforementioned changes was shown by Lea *et al.* (2022) to be good after the first 6 months of ensemble spin-up for all the observed variables.

2.4 | Experimental set-up

Experiments were run for the period December 1, 2019, to end of February 2020. The system runs 44 ensemble members on each 6 hr cycle with forecasts out to 12 hr. Longer forecasts out to 8 days are carried out, but for only 18 members on each 6 hr cycle. The number of ensemble members was chosen to reflect that used in the operational NWP system, where 44 members were found to be the best compromise between accuracy and cost (Bowler *et al.*, 2017a, 2017b). Initial conditions for the ocean–sea-ice ensemble on December 1 were taken from an uncoupled ocean–sea-ice ensemble that had been run for about 21 months. The first portion of the experiment is the same as described by Lea *et al.* (2022) (experiment *ensda08_inf08* in that article) and the experiment was continued on to December 1, 2019, to provide initial conditions for these experiments. That ensemble consisted of only 36 members, so we initialised the ocean parts of members 37–44 of the new ensemble using the first eight members of the ocean–sea-ice ensemble. The atmospheric initial conditions were taken from the operational MOGREPS-G ensemble. All the standard observation types assimilated operationally in atmosphere, land, ocean, and sea-ice components were assimilated in these experiments.

2.5 | Calculation of atmosphere–ocean cross-correlations

We examine instantaneous (zero-lag) cross-correlations between atmospheric (MetUM) and oceanic (NEMO) fields from the ensemble coupled forecasts for December 2019 to February 2020. MetUM and NEMO exchange fields every hour to represent the diurnal cycle of surface fluxes and sea-surface temperature (SST); the forecasts are re-initialised each day at 0000, 0600, 1200, and 1800 UTC, allowing evaluation of the effects of the diurnal cycles as a function of start time. To calculate the correlations we take the difference between each of the 44 ensemble members

and the ensemble mean as a proxy for forecast errors (Bannister, 2008). The correlations of these errors are calculated between different variables at the same horizontal position. For MetUM output, we used 1.5 m air temperature, mean-sea-level pressure, and wind components at 10 m above the sea surface, as well as atmospheric temperature and wind components on pressure levels (nine levels in the troposphere between 1,000 and 200 hPa). For NEMO output, we used upper ocean potential temperature on the NEMO vertical grid (33 levels in the top ~245 m), mixed-layer depth (MLD—from the Kara diagnostic based on a variable density threshold), net heat flux into the ocean (Qnet), net short-wave flux (Qsw), and precipitation (P); net long-wave radiation and latent and sensible heat fluxes are not available in the Met Office archive. The MetUM output files were saved at lower resolution than the NEMO output files. We use an area-weighted linear interpolation to regrid all NEMO data onto the MetUM output grid of 0.5625° longitude × 0.3750° latitude, which is approximately $62.5 \times 42 \text{ km}^2$ at the Equator; all diagnostics shown in this article are performed on this common grid. We analysed correlations on consecutive 5-day intervals for the period December 5, 2019, to February 8, 2020. Daily mean correlations are calculated using the 44 ensemble members from four different forecast start times, giving a sample size of 176. When we consider the diurnal cycle in Section 3.2 we use the 44 members at each start time separately. We focus our results on forecasts for December 15, 2019, initially, before investigating the synoptic variability in the results for different days.

3 | RESULTS

We now present the results of the correlation calculations from the six-hourly forecasts, beginning with correlations between SST and surface meteorology, such as wind speed and air temperature, surface fluxes and MLD. We use the ensemble means of SST and surface meteorology to assist in interpretation of the correlations. Taking the SST and wind speed correlation, we look at its variation over the diurnal cycle and synoptic time-scales. We use atmospheric surface pressure to indicate the synoptic situation. We then move on to inspecting the vertical structure of ocean temperature and wind speed correlation upward into the troposphere and downward into the ocean.

3.1 | Correlation of SST with surface meteorology

In this section we examine the effect of NEMO SST on near-surface meteorological variables used in the

bulk formulas in the MetUM for modelling the air–sea fluxes. Figure 1 shows daily-mean correlations of SST to near-surface meteorological variables, surface fluxes and MLD for six-hourly coupled forecasts initialised on December 15, 2019, using anomalies from the ensemble mean on each cycle and then averaged to give a daily-mean value. Figure 2 shows the corresponding ensemble-mean forecast conditions upon which the anomalies depend averaged over the same day. Significant negative correlations of SST with 10 m wind speed (Figure 1a) over most of the tropical Indian and west Pacific oceans are roughly collocated with the warmest SSTs (Figure 2a) and local 10 m wind speed minima (Figure 2b). As in Frolov *et al.* (2021), there is some evidence that these correlations are associated with large precipitation amounts. Here, we find the strongest correlations in the southern Indian Ocean, to the north and east of Madagascar, where there are strong gradients in the mean precipitation field (see Figure 2d). Large negative correlations also occur over ice-covered areas in high southern latitudes (see Figure 2f). Significant positive correlations occur in localised regions of strong SST gradients, as has previously been noted in the literature (Frolov *et al.*, 2021). Here, we see such correlations along the warm side of the Gulf Stream after separation at Cape Hatteras, which also coincides with an area of strong winds (see Figure 2b). Strong correlations are not seen in other western boundary current regions, most likely due to the low wind speeds in these areas on this specific day. The variation of correlations with synoptic situation will be further discussed in Section 3.3.

Correlations of SST with 1.5 m air temperature (Figure 1b) are positive almost everywhere globally, reflecting the tight coupling between SST and near-surface air temperature anomalies. This occurs particularly over areas where SST is cooler than the air temperature, causing convective overturning and entrainment, higher wind speed (Figure 2b), mixing of the ocean, and finally deepening of the MLD (Figure 2e).

Turning to correlations with surface heat fluxes, correlations between SST and Qnet (defined as positive into the ocean, Figure 1e) are negative in the Northern Hemisphere, particularly over the western boundary current regions, where there is a net flux out of the ocean (Figure 2c). In these areas the SST is warmer than the air temperature and the correlations indicate a negative feedback, where positive SST anomalies increase the air–sea temperature gradient, leading to more heat loss from the ocean. By contrast, over much of the Indo-Pacific Warm Pool, correlations of SST with Qnet follow, to a close approximation, positive correlations with Qsw (Figure 1c), such that the atmosphere drives the SST variability. Correlations of SST with precipitation (Figure 1d) are found to be small overall, with some negative correlations over
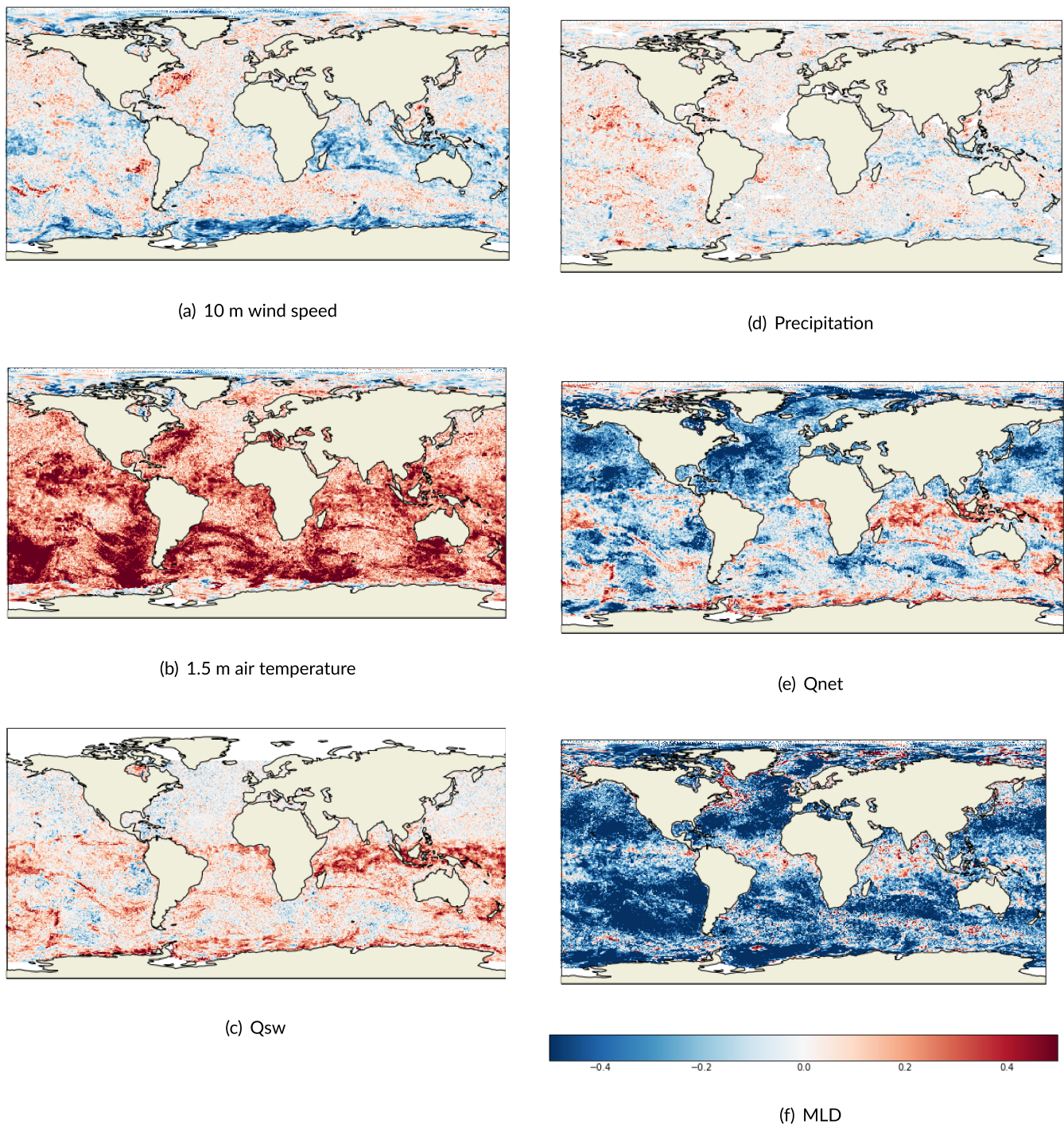
(a) 10 m wind speed

(b) 1.5 m air temperature

(c) Qsw

(d) Precipitation

(e) Qnet

(f) MLD

FIGURE 1   Daily-averaged correlations between NEMO sea-surface temperature (top-level potential temperature over surface layer of ~1 m thickness) and (a) 10 m wind speed, (b) 1.5 m air temperature, (c) net short-wave flux (Qsw), (d) precipitation, (e) net surface heat flux into the ocean (Qnet, defined as positive into the ocean), and (f) mixed-layer depth (MLD), all computed from six-hourly forecast anomalies (relative to the ensemble-mean) and then averaged over December 15, 2019.

the Indian Ocean and the Indo-Pacific Warm Pool, and positive correlations in the eastern Pacific. The negative correlations are approximately aligned with positive correlations with Qsw (Figure 1c), reflecting the strong relationship between radiative and precipitation fluxes. Further, correlations between SST and MLD (Figure 1f) are positive

over much of the Tropics, along the edge of the Labrador Sea, and in parts of the Antarctic Circumpolar Current. The positive correlation corresponds to higher surface current speed, which suggests changes in surface fluxes and upper ocean vertical mixing (involving only vertical processes), as well as contributions from ocean dynamic
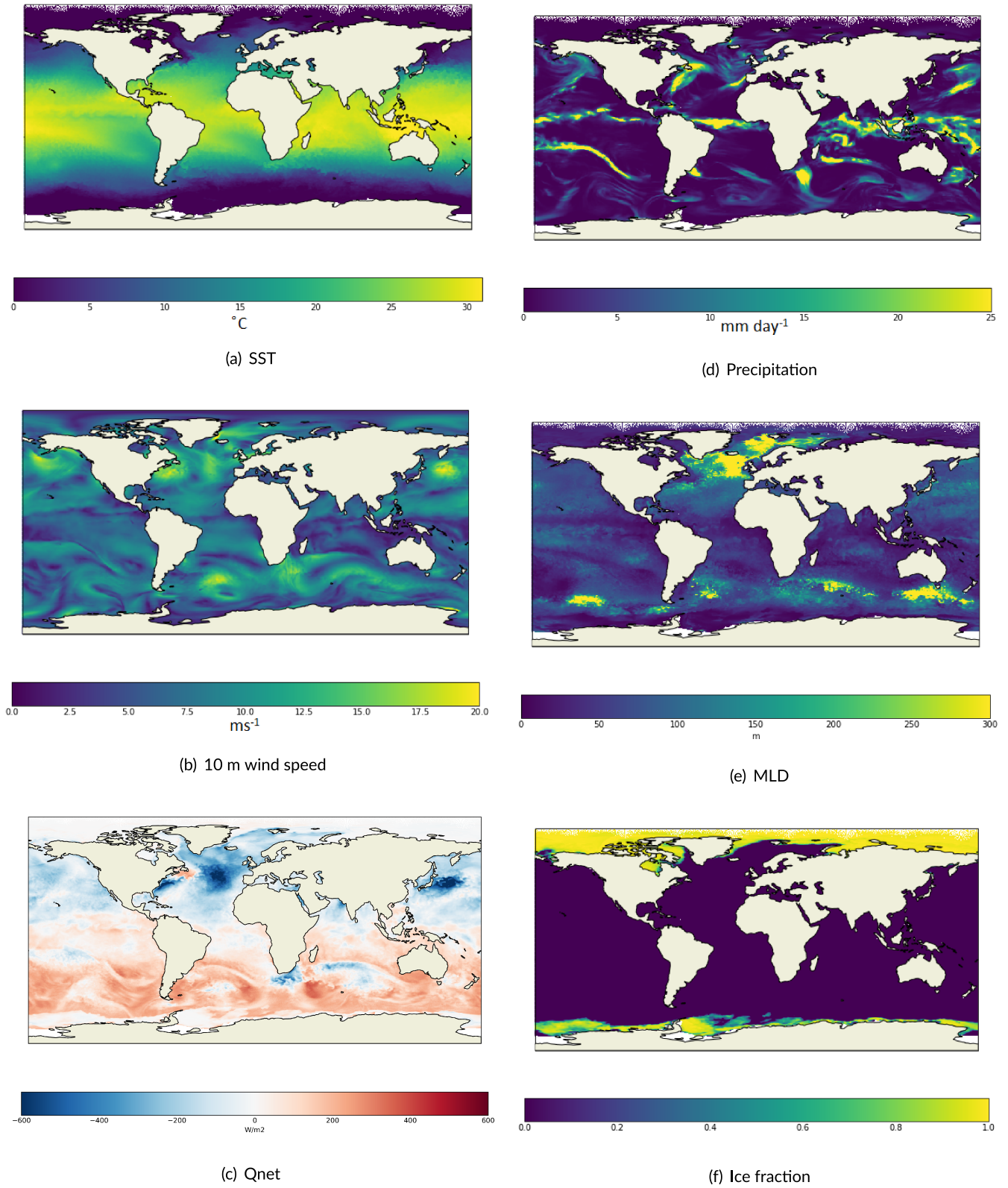
FIGURE 2   Ensemble-mean (a) sea-surface temperature (SST), (b) 10 m wind speed, (c) net surface heat flux into the ocean (Qnet), (d) precipitation, (e) isopycnal mixed-layer depth (MLD), and (f) ice fraction, for six-hourly coupled forecasts averaged over December 15, 2019.

processes represented in NEMO (horizontal and vertical heat transports).

3.2 | Effects of the diurnal cycle

Having considered the daily average correlations, we now examine how the correlations between SST and 10 m wind speed change over the diurnal cycle. Figure 3 shows correlations of SST with 10 m wind speed and net short-wave radiation for each of the four start times used on December 15, 2019, where the labels of the subfigures indicate the validity time of the 6 hr forecast. We see a sub-daily variability of these correlations, which is mainly driven by the diurnal cycle of SST and surface heat fluxes, particularly the diurnal progression of solar radiation, the only term to heat the ocean. Figure 3a–d shows the development of negative SST–wind speed correlations throughout the day, starting in the central and western Pacific (Figure 3a) and gradually spreading to the Indian Ocean (Figure 3b,c). These are collocated with strong positive correlations between SST and Qsw over the tropical oceans (Figure 3e–h). In each of these regions the correlations strengthen as the solar radiation varies from zero at night (local time) to a maximum insolation (modulated by the effect of clouds) from midday and into the afternoon (local time). For example, in the Indian Ocean, negative correlations of SST with 10 m wind speed strengthen throughout the day, increasing from 0600 UTC (local noon, Figure 3b) and throughout the afternoon to 1200 UTC (1800 h local time). Overall, the largest SST–wind speed correlations are associated with maximum insolation and positive correlations with Qsw. These negative correlations are largest (< -0.5) in the western Indian Ocean and around the Maritime Continent in the West Pacific. This is a consequence of the shallow mixed layer (10 to ∼30 m; Figure 2e), which allows a faster response to solar heating. Finally, we note that the positive correlations over the Gulf Stream region do not exhibit any variation with the diurnal cycle and are not associated with significant correlations between SST and Qsw. These correlations do not arise from the effect of variations in solar radiation, but rather from the synoptic situation. We now investigate this in more depth.

3.3 | Synoptic variability

In this section we demonstrate how the correlations between SST and 10 m wind speed vary on synoptic time-scales on consecutive 5-day intervals. There are significant variations in correlation intensities and structures in response to the synoptic time-scale forcing. Figure 4 shows synoptic variability maps of daily-mean correlations

between SST and 10 m wind speed from December 5, 2019, to February 8, 2020 (sampled every 5 days), with the contour lines corresponding to large-scale patterns in mean-sea-level atmospheric surface pressure over the same period. Significant positive correlations are present in the western North Atlantic from early to mid December (Figure 4a–c), on January 9 (Figure 4h), and at the end of the period (Figure 4n), which are either absent or weaker in this area on other days (Figure 4d–g,i–m). These are all associated with large gradients in surface pressure and the associated high wind speeds, which advect cold, dry continental air eastward over the warmer Atlantic Ocean. At high southern latitudes, significant positive correlations develop to the north of cyclonic storms that track eastward around Antarctica and frequently become more intense due to strong meridional SST gradients (between ice and open ocean); this can be seen in late December and early January in the southeast Indian Ocean, in the area southwest of Australia, and in the southern Pacific Ocean west of the coast of Patagonia (Figure 4e–h,j,k).

Finally, changes in correlation intensities in the Tropics are primarily associated with variability in strength of the subtropical high-pressure belts that drive trade winds towards the lower pressure zone at the Equator; significant negative correlations across the Indo-Pacific Warm Pool are always associated with light wind conditions (i.e., wind speeds <5 m·s^{-1}, as shown in Figure 2b for the December 15 case).

3.4 | Vertical extent of correlation structures in atmosphere and ocean

Within DA, as well as specifying multivariate relationships, covariance information is also used to spread information spatially. We now, therefore, examine the vertical structure of the daily-mean correlations between SST and the low-level atmospheric temperature and winds, and between the 10 m wind and upper ocean temperatures. Figure 5a–c shows patterns of correlations between SST and tropospheric wind speeds on three different pressure levels. At 1,000 hPa (Figure 5a) the correlations are similar to those for 10 m winds (Figure 1a), as would be expected. The strong negative correlations over the Indian Ocean and the Southern Ocean are still present at 925 hPa, but correlation magnitudes are noticeably weaker at 850 hPa. This is explained by the fact that SST variability has little effect on mid and upper tropospheric circulation above the atmospheric boundary layer. Correlations between SST and 1,000 hPa air temperature (Figure 5d) reproduce a similar pattern of positive correlations to that obtained for 1.5 m air temperature (Figure 1b), but with lower amplitudes; this is particularly noticeable
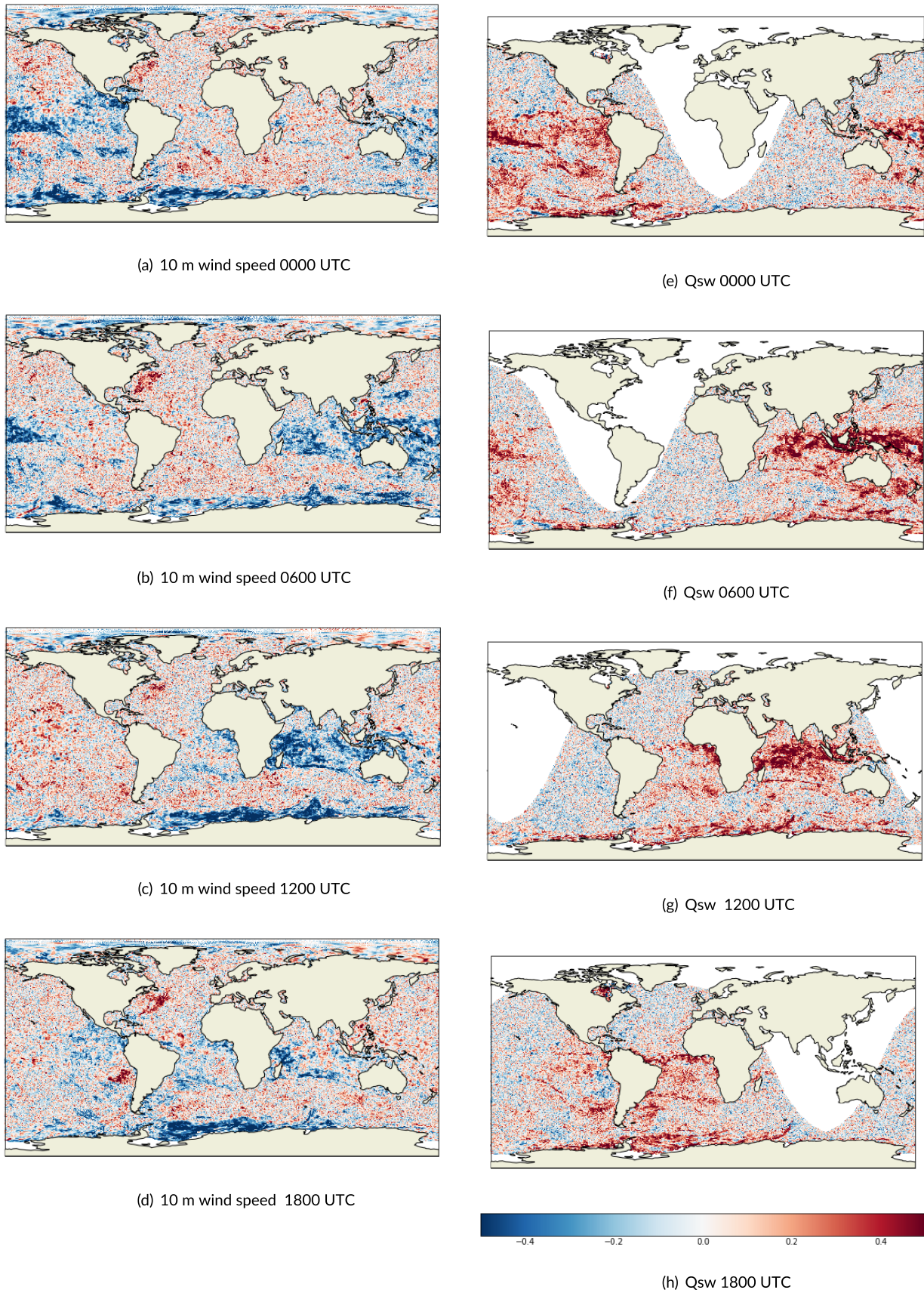
(a) 10 m wind speed 0000 UTC

(b) 10 m wind speed 0600 UTC

(c) 10 m wind speed 1200 UTC

(d) 10 m wind speed 1800 UTC

(e) Qsw 0000 UTC

(f) Qsw 0600 UTC

(g) Qsw 1200 UTC

(h) Qsw 1800 UTC

FIGURE 3 Correlations between sea-surface temperature and (a–d) 10 m wind speed and (e–h) net short-wave radiation (Qsw) as a function of the validity time of the six-hourly forecast (i.e., 0000, 0600, 1200, and 1800 UTC) on December 15, 2019.
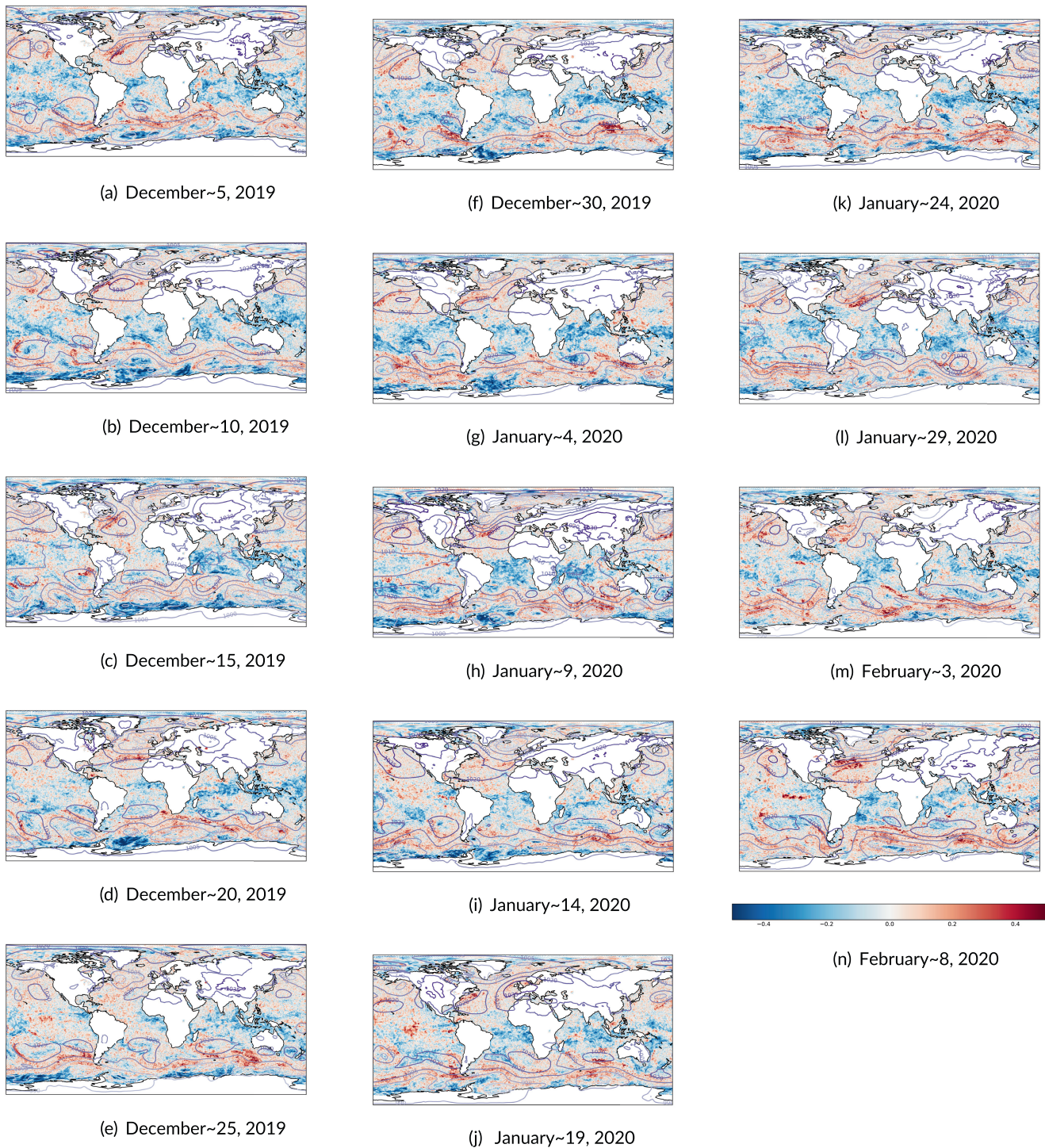
FIGURE 4 Daily-mean correlations of sea-surface temperature and 10 m wind speed on consecutive 5-day intervals from December 5, 2019, to February 8, 2020, with contour lines corresponding to the the daily ensemble-mean sea-level atmospheric surface pressure field. (a) December 5, 2019; (b) December 10, 2019; (c) December 15, 2019; (d) December 20, 2019; (e) December 25, 2019; (f) December 30, 2019; (g) January 4, 2020; (h) January 9, 2020; (i) January 14, 2020; (j) January 19, 2020; (k) January 24, 2020; (l) January 29, 2020; (m) February 3, 2020; (n) February 8, 2020.

over the Antarctic Circumpolar Current into the southern Pacific and Atlantic oceans, and in the western North Atlantic Gulf Stream region. There is a lack of significant correlations at levels above 1,000 hPa (Figure 5e,f).

In previous idealised studies in a single-column model (Smith *et al.*, 2017) we found that correlations existed up to the top of the atmospheric boundary layer. Here, it is possible that the average boundary-layer height over the
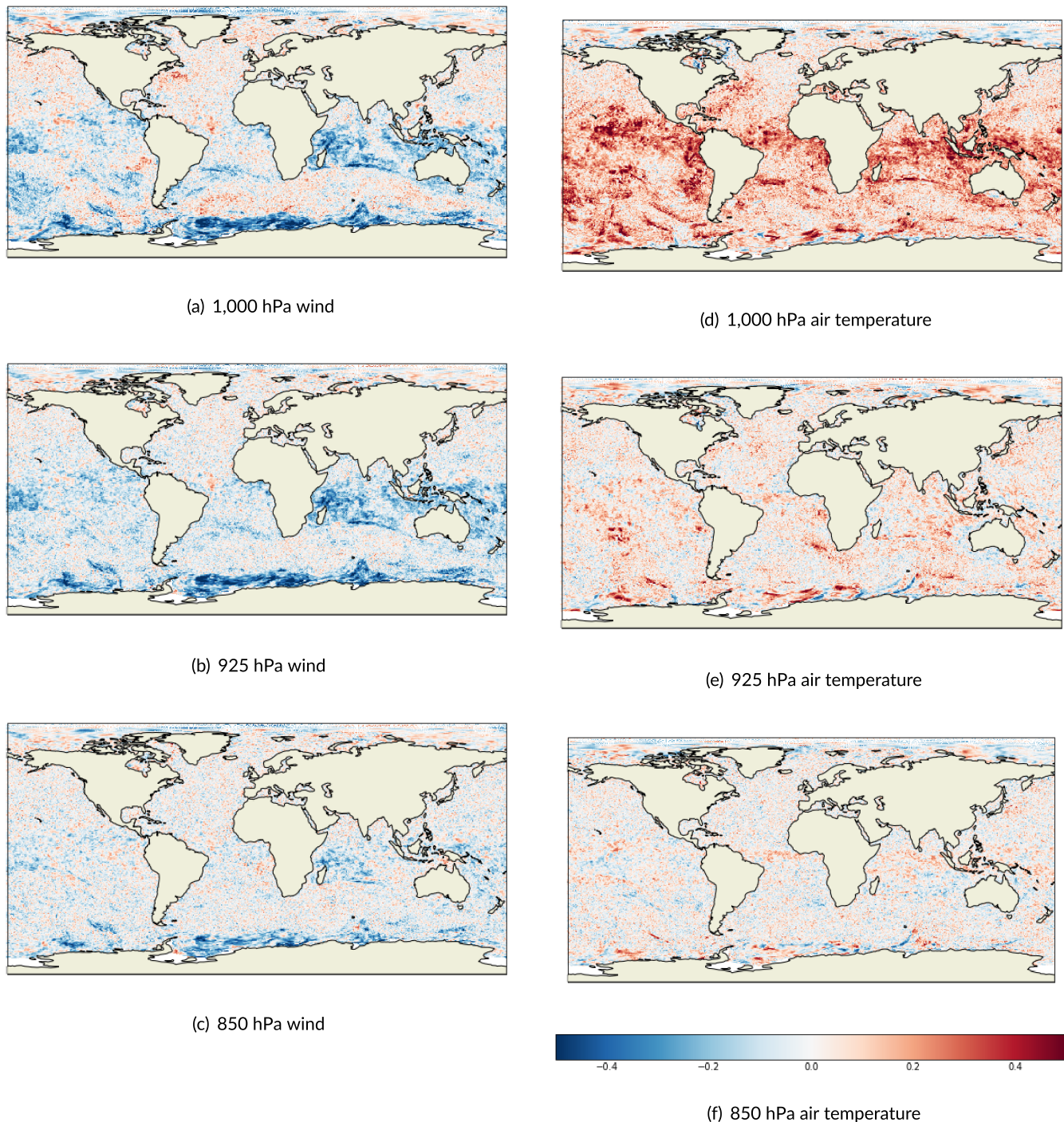
FIGURE 5 Spatial maps of daily-mean correlations between sea-surface temperature and tropospheric (a–c) wind speed and (d–f) air temperature as a function of pressure level (1,000–850 hPa), for six-hourly forecasts initialised on December 15, 2019: (a) 1,000 hPa wind; (b) 925 hPa wind; (c) 850 hPa wind; (d) 1,000 hPa air temperature; (e) 925 hPa air temperature; (f) 850 hPa air temperature.

day is generally below 925 hPa or that there is insufficient atmospheric vertical resolution in MetUM to generate fine-scale vertical structure in air temperature anomalies.

Figure 6 shows the corresponding daily-mean correlations of 10 m wind speed with upper ocean temperature at different depths, from 0.51 m down to 244.89 m. In

Figure 6a–e we show the correlations for December 15, 2019. In the Gulf Stream region, positive correlations between wind speed and subsurface ocean temperatures are generally vertically coherent up to a depth of over 100 m, with a small signal still remaining at 244 m. As discussed in Section 3.3, these positive correlations are
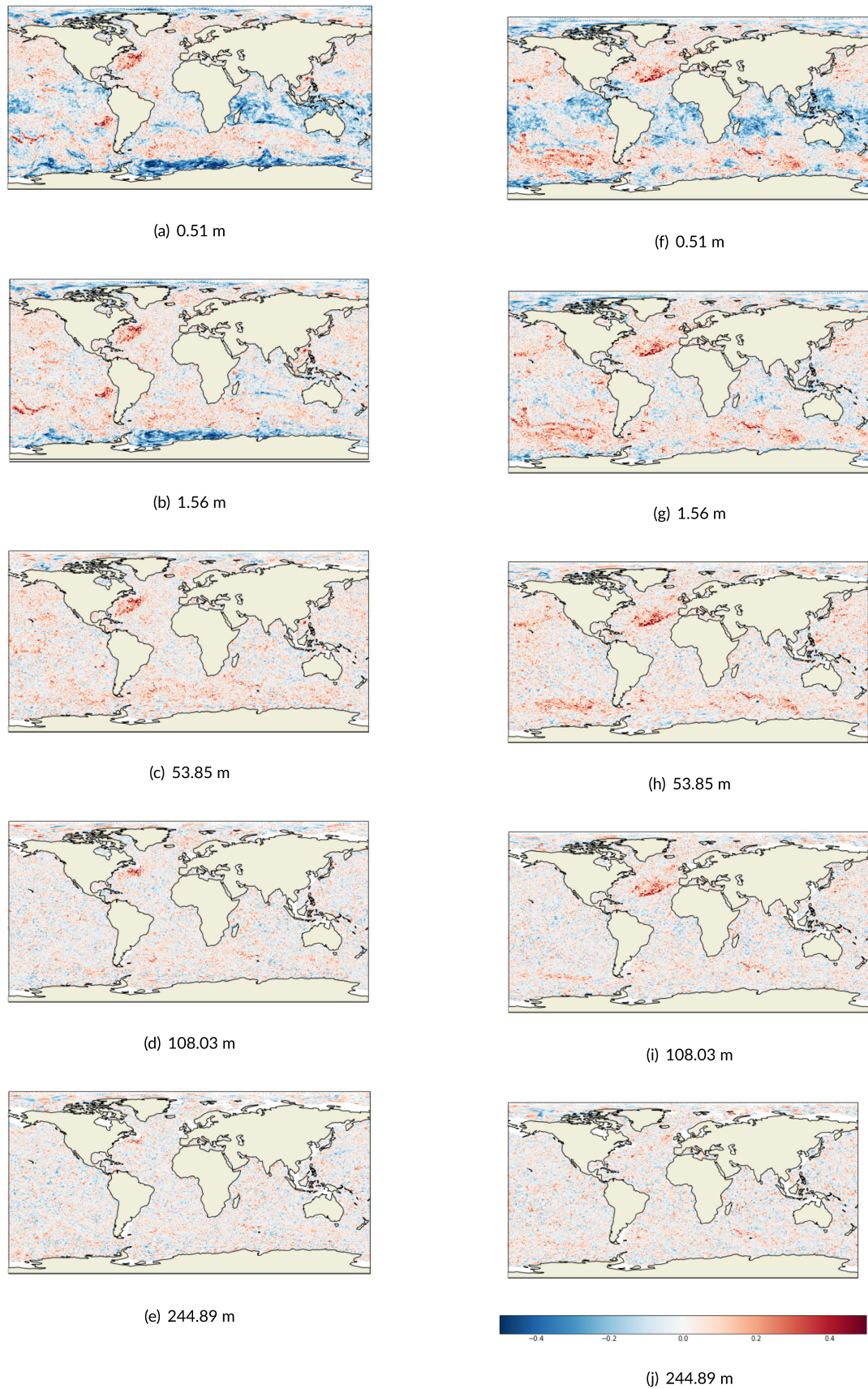
FIGURE 6 Spatial maps of daily-mean correlations between 10 m wind speed anomalies and upper ocean temperature anomalies at different depths, for six-hourly forecasts initialised on (a–e) December 15, 2019, and (f–j) January 29, 2020: (a) 0.51 m; (b) 1.56 m; (c) 53.85 m; (d) 108.03 m; (e) 244.89 m; (f) 0.51 m; (g) 1.56 m; (h) 53.85 m; (i) 108.03 m; (j) 244.89 m.

associated with strong winds around a low-pressure system, which lead to a well-mixed ocean and a deep mixed layer, as shown in Figure 2e. This means that the effect of the wind on the ocean surface is felt all the way through the deep mixed layer. However, in the tropical Indian and West Pacific oceans, negative correlations found in Figure 6a break down just below the surface layer ($\sim$1 m thick). Though such an effect could be caused by the presence of salinity-stratified boundary layers that form in these areas, further investigation shows that this is not the case here, and the barrier layer thickness is relatively large in these areas. Instead, the shallow correlation structures are likely due to the very shallow mixed layer in those areas (see Figure 2e), with the top layer of the ocean reacting to the diurnal cycle of solar radiation, as discussed in Section 3.2, but with no possibility of this effect feeding deeper into the ocean. In order to understand whether these conclusions also hold on a different date, we plot correlations on the same depths for January, 29 2020, in Figure 6f–j. On this date we see the same pattern. There are positive correlations in the North Atlantic, this time away from the Gulf Stream area and associated with a different synoptic system (see Figure 4l), which extend beyond 100 m depth. Again, in the Indian and western Pacific oceans, there are strong negative correlations that are present only at the surface. We note that strong negative correlations between the 10 m wind and the near-surface ocean temperatures over Antarctica in December (Figure 6a) are not present in January (Figure 6f). Over areas of partial ice cover we expect the air–sea flux to be sensitive to the atmospheric winds. As the winds move the ice around, this affects the size and position of the leads, and hence the strength of the flux in different places, creating the strong correlations seen in December. However, as the melt season progresses into January, the ice concentration becomes lower, and thus the sensitivity of the fluxes to the wind is reduced.

4 | CONCLUSIONS

The aim of this study was to understand the strength and nature of atmosphere–ocean cross-correlations in short-range forecast errors. In particular, we have focused on correlations from 6 hr forecasts, for a Northern Hemisphere winter period. Though it could be of interest to compare correlations for different forecast lengths, the forecast period chosen reflects the DA window of the Met Office system. This allowed us to characterise the correlation structures relevant to the background fields used in practice. Overall, the results have shown that significant correlations exist between atmosphere and ocean forecast errors on these short time-scales. This indicates a potential benefit from including cross-correlation information in CDA systems.

When we examined the nature of these cross-correlations, we found that they vary diurnally, from day to day, spatially and synoptically. The evaluation of cross-correlations between SST and surface meteorology fields showed significant positive correlations of SST with 10 m wind speed in the North Atlantic, associated with strong SST gradients. Such signals have previously been noted in averaged correlations (e.g., Frolov *et al.*, 2021). Here, we have seen how these positive correlations are synoptically dependent and tend to be associated with areas of stronger winds. Furthermore, they extend vertically into the ocean, throughout the mixed layer, which can be quite deep in these situations.

Over the Indian and western Pacific oceans we found negative correlations between SST and 10 m wind speed, associated with warm SST and low wind speeds. These were not synoptically dependent, but were instead linked to diurnal variations in solar radiation, with correlations strengthening as the ocean surface heated throughout the day. These correlations were in locations of shallow mixed layers and remained at the surface, with no penetration into the ocean, disappearing during the local night.

Overall, the variability in the atmosphere–ocean cross-correlations seen indicates that using flow-dependent correlations could be key to their effectiveness when including them in CDA systems. Furthermore, the differing vertical extents of the correlations found in Section 3.4 imply that the length scales used in the vertical localisation of ensemble correlations would need to be situation dependent, so as to remove noise at long distances where the correlations are shallow, while retaining genuine deep correlations. The question of how to implement such schemes in practice should be the focus of further research.

DATA AVAILABILITY STATEMENT

ORCID

Amos S. Lawless https://orcid.org/0000-0002-3016-6568
Nancy K. Nichols https://orcid.org/0000-0003-1133-5220
Daniel J. Lea https://orcid.org/0000-0003-1736-628X
Matthew J. Martin https://orcid.org/0000-0003-0293-3106

REFERENCES

Bannister, R.N. (2008) A review of forecast error covariance statistics in atmospheric variational data assimilation. I: characteristics and measurements of forecast error covariances. *Quarterly Journal of the Royal Meteorological Society*, 134, 1951–1970. Available from: https://doi.org/10.1002/qj.339

Bloom, S. C., Takacs, L. L., da Silva, A. M., & Ledvina, D. (1996) Data assimilation using incremental analysis updates. *Monthly Weather Review*, 124(6), 1256–1271. Available from: https://doi.org/10.1175/1520-0493(1996)124<1256:dauiau>2.0.co;2

Bowler, N.E., Clayton, A.M., Jardak, M., Jermey, P.M., Lorenc, A.C., Wlasak, M.A. et al. (2017a) The effect of improved ensemble covariances on hybrid variational data assimilation. *Quarterly Journal of the Royal Meteorological Society*, 143, 785–797. Available from: https://doi.org/10.1002/qj.2964

Bowler, N.E., Clayton, A.M., Jardak, M., Lee, E., Lorenc, A.C., Piccolo, C. et al. (2017b) Inflation and localization tests in the development of an ensemble of 4D-ensemble variational assimilations. *Quarterly Journal of the Royal Meteorological Society*, 143, 1280–1302. Available from: https://doi.org/10.1002/qj.3004

Browne, P., de Rosnay, P., Zuo, H., Bennet, A. & Dawson, A. (2019) Weakly coupled ocean–atmosphere data assimilation in the ECMWF NWP system. *Remote Sensing*, 11(3), 234. Available from: https://doi.org/10.3390/rs11030234

Craig, A., Valcke, S., & Coquart, L. (2017) Development and performance of a new version of the OASIS coupler, OASIS3-MCT_3.0. *Geoscientific Model Development*, 10(9), 3297–3308. Available from: https://doi.org/10.5194/gmd-10-3297-2017

de Rosnay, P., Browne, P., de Boisséson, E., Fairbairn, D., Hirahara, Y., Ochi, K. et al. (2022) Coupled data assimilation at ECMWF: current status, challenges and future developments. *Quarterly Journal of the Royal Meteorological Society*, 148, 2672–2702. Available from: https://doi.org/10.1002/qj.4330

Frolov, S., Reynolds, C.A., Alexander, M., Flatau, M., Barton, N.P., Hogan, P. et al. (2021) Coupled ocean–atmosphere covariances in global ensemble simulations: impact of an Eddy-resolving ocean. *Monthly Weather Review*, 149, 1193–1209. Available from: https://doi.org/10.1175/MWR-D-20-0352.1

Gómez, B., Charlton-Pérez, C.L., Lewis, H. & Candy, B. (2020) The Met Office operational soil moisture analysis system. *Remote Sensing*, 12, 3691. Available from: https://doi.org/10.3390/rs12223691

Guiavarc'h, C., Roberts-Jones, J., Harris, C., Lea, D.J., Ryan, A. & Ascione, I. (2019) Assessment of ocean analysis and forecast from an atmosphere-ocean coupled data assimilation operational system. *Ocean Science*, 15, 1307–1326. Available from: https://doi.org/10.5194/os-15-1307-2019

Houtekamer, P.L. & Zhang, F. (2016) Review of the ensemble Kalman filter for atmospheric data assimilation. *Monthly Weather Review*, 144, 4489–4532. Available from: https://doi.org/10.1175/MWR-D-15-0440.1

Inverarity, G.W., Tennant, W.J., Anton, L., Bowler, N.E., Clayton, A.M., Jardak, M. et al. (2023) Met Office MOGREPS-G initialisation using an ensemble of hybrid four-dimensional ensemble variational (En-4DEnVar) data assimilations. *Quarterly Journal of the Royal Meteorological Society*, 149, 1138–1164. Available from: https://doi.org/10.1002/qj.4431

Laloyaux, P., Frolov, S., Ménétrier, B. & Bonavita, M. (2018) Implicit and explicit cross-correlations in coupled data assimilation. *Quarterly Journal of the Royal Meteorological Society*, 144, 1851–1863. Available from: https://doi.org/10.1002/qj.3373

Lea, D.J., Martin, M., Price, M., Robert-Jones, J., Tennat, W. & Harris, C. (2023) Assessing the impact of including a global ocean ensemble system in the Met Office coupled numerical weather prediction system. *Met Office Forecasting Research Technical Report*, 657, 55.

Lea, D.J., Mirouze, I., Martin, M.J., King, R.R., Hines, A., Walters, D. et al. (2015) Assessing a new coupled data assimilation system based on the Met Office coupled atmosphere-land-ocean-sea ice model. *Monthly Weather Review*, 143, 4678–4694. Available from: https://doi.org/10.1175/MWR-D-15-0174.1

Lea, D.J., While, J., Martin, M.J., Weaver, A., Storto, A. & Chrust, M. (2022) A new global ocean ensemble system at the Met Office: assessing the impact of hybrid data assimilation and inflation settings. *Quarterly Journal of the Royal Meteorological Society*, 148, 1996–2030. Available from: https://doi.org/10.1002/qj.4292

Lorenc, A.C., Jardak, M., Payne, T., Bowler, N.E. & Wlasak, M.A. (2017) Computing an ensemble of variational data assimilations using its mean and perturbations. *Quarterly Journal of the Royal Meteorological Society*, 143, 798–805. Available from: https://doi.org/10.1002/qj.2965

Mirouze, I., Blockley, E.W., Lea, D.J., Martin, M.J. & Bell, M.J. (2016) A multiple length scale correlation operator with application to ocean data assimilation. *Tellus A*, 68, 29744. Available from: https://doi.org/10.3402/tellusa.v68.29744

Ollinaho, P., Lock, S.-J., Leutbecher, M., Bechtold, P., Beljaars, A., Bozzo, A. et al. (2017) Towards process-level representation of model uncertainties: stochastically perturbed parametrizations in the ECMWF ensemble. *Quarterly Journal of the Royal Meteorological Society*, 143, 408–422. Available from: https://doi.org/10.1002/qj.2931

Piccolo, C., Cullen, M.J.P., Tennant, W.J. & Semple, A.T. (2019) Comparison of different representations of model error in ensemble forecasts. *Quarterly Journal of the Royal Meteorological Society*, 145, 15–27. Available from: https://doi.org/10.1002/qj.3348

Ridley, J.K., Blockley, E.W., Keen, A.B., Rae, J.G.L., West, A.E. & Schroeder, D. (2018) The sea ice model component of

HadGEM3-GC3.1. *Geoscience Model Development*, 11, 713–723. Available from: https://doi.org/10.5194/gmd-11-713-2018

Sanchez, C., Williams, K.D. & Collins, M. (2016) Improved stochastic physics schemes for global weather and climate models. *Quarterly Journal of the Royal Meteorological Society*, 142, 147–159. Available from: https://doi.org/10.1002/qj.2640

Smith, P.J., Fowler, A.M. & Lawless, A.S. (2015) Exploring strategies for coupled 4D-Var data assimilation using an idealised atmosphere–ocean model. *Tellus A: Dynamic Meteorology and Oceanography*, 67, 1. Available from: https://doi.org/10.3402/tellusa.v67.27025

Smith, P.J., Lawless, A.S. & Nichols, N.K. (2017) Estimating forecast error covariances for strongly coupled atmosphere-ocean 4D-Var data assimilation. *Monthly Weather Review*, 145, 4011–4035. Available from: https://doi.org/10.1175/MWR-D-16-028

Smith, P.J., Lawless, A.S. & Nichols, N.K. (2018) Treating sample covariances for use in strongly coupled atmosphere-ocean data assimilation. *Geophysical Research Letters*, 45, 445–454. Available from: https://doi.org/10.1002/2017GL075534

Smith, P.J., Lawless, A.S. & Nichols, N.K. (2020) The role of cross-domain error correlations in strongly coupled 4D-Var atmosphere–ocean data assimilation. *Quarterly Journal of the Royal Meteorological Society*, 146, 2450–2465. Available from: https://doi.org/10.1002/qj.3802

Storkey, D., Blaker, A.T., Mathiot, P., Megann, A., Aksenov, Y., Blockley, E.W. et al. (2018) UK Global Ocean GO6 and GO7: a traceable hierarchy of model resolutions. *Geoscientific Model Development*, 11, 3187–3213. Available from: https://doi.org/10.5194/gmd-11-3187-2018

Storto, A. & Andriopoulos, P. (2021) A new stochastic ocean physics package and its application to hybrid-covariance data assimilation. *Quarterly Journal of the Royal Meteorological Society*, 147, 1691–1725. Available from: https://doi.org/10.1002/qj.3990

Tennant, W. & Beare, S. (2014) New schemes to perturb sea-surface temperature and soil moisture content in MOGREPS. *Quarterly Journal of the Royal Meteorological Society*, 140, 1150–1160. Available from: https://doi.org/10.1002/qj.2202

Vellinga, M., Copsey, D., Graham, T., Milton, S. & Johns, T. (2020) Evaluating benefits of two-way ocean–atmosphere coupling for global NWP forecasts. *Weather and Forecasting*, 35, 2127–2144. Available from: https://doi.org/10.1175/WAF-D-20-0035.1

Walters, D., Baran, A.J., Boutle, I., Brooks, M., Earnshaw, P., Edwards, J. et al. (2019) The Met Office unified model global atmosphere 7.0/7.1 and JULES global land 7.0 configurations. *Geoscientific Model Development*, 12, 1909–1963. Available from: https://doi.org/10.5194/gmd-12-1909-2019

Waters, J., Lea, D., Martin, M., Mirouze, I., Weaver, A. & While, J. (2015) Implementing a variational data assimilation system in an operational 1/4 degree global ocean model. *Quarterly Journal of the Royal Meteorological Society*, 141, 333–349. Available from: https://doi.org/10.1002/qj.2388

Whitaker, J.S. & Hamill, T.M. (2012) Evaluating methods to account for system errors in ensemble data assimilation. *Monthly Weather Review*, 140, 3078–3089. Available from: https://doi.org/10.1175/MWR-D-11-00276.1